Environmental Toxicology

WILEY

ENVIRONMENTAL TOXICOLOGY

RESEARCH ARTICLE OPEN ACCESS

Effects of Tributyltin Chloride on Human Neuronal Differentiation and Mice Brain Development

Ester López-Gallardo[1,2,3] | Patricia Meade[1,2,3,4] | Irene Jiménez-Salvador[1,2] | Carmen Hernández-Ainsa[1,2] | Eldris Iglesias[1,2] | Alba Pesini[1,2] | Nuria Garrido-Pérez[1,2,3,4] | Sonia Emperador[1,2,3] | David Pacheu-Grau[1,2,3] | Pilar Bayona-Bafaluy[1,2,3,4] | Eduardo Ruiz-Pesini[1,2,3]

[1]Departamento de Bioquímica, Biología Molecular y Celular, Universidad de Zaragoza, Zaragoza, Spain | [2]Instituto de Investigación Sanitaria (IIS) de Aragón, Zaragoza, Spain | [3]Centro de Investigaciones Biomédicas en Red de Enfermedades Raras (CIBERER), Instituto de Salud Carlos III (ISCIII), Madrid, Spain | [4]Instituto de Biocomputación y Física de Sistemas Complejos (BIFI), Universidad de Zaragoza, Zaragoza, Spain

Correspondence: Ester López-Gallardo (esterlop@unizar.es) | Eduardo Ruiz-Pesini (eduruiz@unizar.es)

Received: 8 May 2025 | **Revised:** 12 November 2025 | **Accepted:** 31 December 2025

Keywords: brain development | mitochondria | neuronal differentiation | oxidative phosphorylation | perinatal exposure | tributyltin

ABSTRACT

According to the developmental origins of health and disease hypothesis, perinatal exposure to an environmental toxicant during the development of the nervous system could cause a permanent cellular modification that may promote the appearance of neurodegenerative diseases at an older age. Tributyltin chloride is an environmental pollutant that, among other effects, provokes a dysfunction of the oxidative phosphorylation system and has adverse effects on the nervous system. We studied neuronal differentiation of human neuroblastoma cells and neural stem cells in the presence of tributyltin chloride concentrations found in human blood (≤100 nM), and brain development in two-year-old mice after perinatal exposure to tributyltin chloride (≤1000 nM). Pregnant mice (8–9 weeks old) were exposed to TBTC (0, 100, 500, or 1000 nM) via drinking water throughout gestation and lactation and ended upon weaning of the pups. Genetic-molecular, biochemical and cellular studies were performed on human SH-SY5Y neuroblastoma cells and on neural stem cells differentiating into neurons. In addition to these studies, histological studies of the brain and functional tests were performed in two-year-old mice. A decrease in the oxidative phosphorylation activity, essential for the proper function of the nervous system, affected neuronal differentiation of human neural stem cells and neuroblastoma cells in vitro. Exposure to this compound during pregnancy and lactation resulted in a modification of global deoxyribonucleic acid methylation levels in 2-year-old mice. Additionally, various histological changes were detected in the brains of these mice. Therefore, the alteration of brain development with long-term consequences may be one of the manifestations of early exposure to tributyltin.

1 | Introduction

Tributyltin (TBT) was extensively utilized as a biocide in antifouling paints, among other applications. Its widespread use and slow breakdown in the environment have led to significant contamination of human food and water sources [1]. In fact, various studies have detected TBT concentrations in human blood ranging from 8.3 to 293 nM [2]. Due to the off-target effects caused by TBT, its use in paints was globally banned [3]. However, despite efforts to halt the trade of TBT, the production of TBT-based paints continues [4].

The proton channel of adenosine triphosphate (ATP) synthase [complex V (CV) of the oxidative phosphorylation (OXPHOS) system] is a key target for TBT chloride (TBTC) [5]. Animal studies have shown that mitochondrial respiration is significantly reduced in mitochondria from the digestive gland of mussels, ox heart, and mouse or rat liver when treated with TBTC [6–10].

Similarly, in human cell lines such as osteosarcoma 143B, adenocarcinoma A549, and adipose tissue-derived stem cells, oxygen consumption was reduced when exposed to 50–100 nM TBTC [11, 12]. Indeed, significant negative correlations between TBTC concentrations and oxygen consumption were observed in these tumor cells [12]. Previous research demonstrated that TBT at concentrations between 25 and 250 nM reduced ATP levels in human cells like natural killer cells, adrenocortical H295R cells, osteosarcoma 143B, adenocarcinoma A549, embryonic carcinoma NT2/D1, and rat thymocyte [12–16]. Moreover, negative correlations between TBTC levels and ATP concentrations were also significant [12]. In other research, a reduction in mitochondrial inner membrane potential (MIMP) was observed when mouse thymocytes, human adenocarcinoma A549 cells, rat myocytes, and bovine sperm were exposed to 10–100 nM TBT [12, 17–19]. These findings indicate that TBT exerts harmful effects on OXPHOS function at levels found within the human population.

The proper function of the OXPHOS system is essential for neuronal differentiation [20]. Indeed, mutations in genes related to OXPHOS have been shown to impair neuronal differentiation [20]. Additionally, various xenobiotics negatively impact OXPHOS function and neurogenesis by interacting with mitochondrial DNA (mtDNA)-encoded proteins or RNAs [20–22]. Notably, some of these substances affect dopaminergic neurogenesis and heighten the risk of developing Parkinson's disease (PD) [21].

According to the "developmental origins of health and disease" hypothesis, exposure to environmental toxicants during the perinatal period, when the nervous system is developing, could cause permanent cellular changes that promote neurodegenerative diseases in old age [23]. As previously mentioned, TBTC causes OXPHOS system dysfunction, a crucial metabolic pathway in the development of the nervous system. In this study, we expand the investigation of TBTC's impact on the OXPHOS system to other cell types, specifically human SH-SY5Y neuroblastoma cells and neuronal precursor cells, and evaluate its effect on neuronal differentiation. Dopaminergic neurogenesis primarily occurs in humans between weeks 5 and 7 post-fertilization, and in mice between embryonic days 7 and 15 [24]. Therefore, we also examined the effects of early TBTC exposure on aged mice, during which the incidence of PD tends to increase.

2 | Material and Methods

2.1 | Cells, Proliferation Conditions, Neural Differentiation, and Toxicological Treatments

The human neuroblastoma SH-SY5Y cell line was obtained from Sigma (St. Louis, MO, USA, catalog number 94030304, lot 13C014, P 17). Cells were cultured in DMEM low glucose (5 mM), 4 mM L-glutamine, 1 mM sodium pyruvate and supplemented with 10% fetal bovine serum (FBS). To induce neural differentiation, SH-SY5Y cells were seeded in culture dishes; 24 h later, medium was replaced with neurobasal-A medium, no D-glucose, no sodium pyruvate (catalog number A2477501, Thermo Fisher Scientific) and supplemented with 5 mM glucose, 1 mM sodium pyruvate, 2% B27, 1% N2, 1% Culture One, 1% GlutaMAX Supplement (Thermo Fisher Scientific), and 10 μM retinoic acid for 7 days.

The human induced pluripotent stem cells (hiPSCs) were obtained from a healthy donor [25]. To induce human neural stem cells (hNSCs), hiPSCs were cultured for 7 days using Gibco PSC Neural Induction Medium (Thermo Fisher Scientific, Waltham, MA), according to the manufacturer's instructions. The culture medium was replaced on day 6 to Neural Expansion Medium that was kept up to day 11. Accutase (Millipore, Billerica, MA) cell detachment solution was applied to hNSCs for passaging. hNSCs (< 10 passages) were grown in KnockOut DMEM/F-12 medium containing StemPro Neural Supplement (2%), fibroblast growth factor-basic (FGFb, 20 ng/mL), epidermal growth factor (EGF, 20 ng/mL), and L-glutamine (2 mM), on cell culture plates previously coated with CellStart. Neural differentiation of hNSCs was induced in polyornithine and laminin-coated culture dishes. hNSCs were cultured for 24 h at 37°C. The neuronal differentiation was then induced by substituting the medium with neurobasal-A medium, no D-glucose, no sodium pyruvate (catalog number A2477501, Thermo Fisher Scientific) supplemented with 5 mM glucose, 1 mM sodium pyruvate, 2% B27, 1% Culture One, 1% GlutaMAX Supplement (Thermo Fisher Scientific), and 200 μM ascorbic acid for 7 days.

For neuronal differentiation in the presence of xenobiotics, SH-SY5Y cells and hNSCs were exposed to TBTC (10, 20, 50, 75, 100 nM) dissolved in ethanol 100% during the 7 days of neural differentiation. Final ethanol concentration in the media did not exceed 0.05%. For other studies of undifferentiated and differentiated cells, exposure to TBTC was carried out for 2–7 days.

2.2 | Animals and Xenobiotic Administration

Male and female C57BL/6J mice (6–7 weeks old) were purchased from Charles River Laboratories (France). Animals were housed in soft filter top cages in a 12 h:12 h light/dark cycle, 55% ± 10% humidity, and 22°C ± 2°C temperature-controlled room, with free access to autoclaved water and irradiated food (2914 Teklad Global 14% protein rodent maintenance diet). All procedures were carried out under Project License PI58/15 approved by the Ethic Committee for Animal Experiments from Universidad de Zaragoza. The care and use of animals were performed in accordance with the Spanish Policy for Animal Protection RD53/2013, which meets the European Union Directive 2010/63 on the protection of animals used for experimental and other scientific purposes.

TBTC was dissolved in ethanol and diluted in 0.5% carboxymethylcellulose in water to maximize solubility. For vehicle solution, a volume of ethanol equal to the largest amount added to the TBTC-containing water solution was added.

The mice were allowed to acclimatize for at least 4 days before use. For mating, 1 male was housed with 2 females for 10 days. Female mice were randomly divided into three treatment groups and one control group (8 females per treatment group) and from 5 days before mating were exposed to TBTC via drinking water. The TBTC concentrations were 0, 100, 500, or 1000 nM, which are realistic environmental exposure

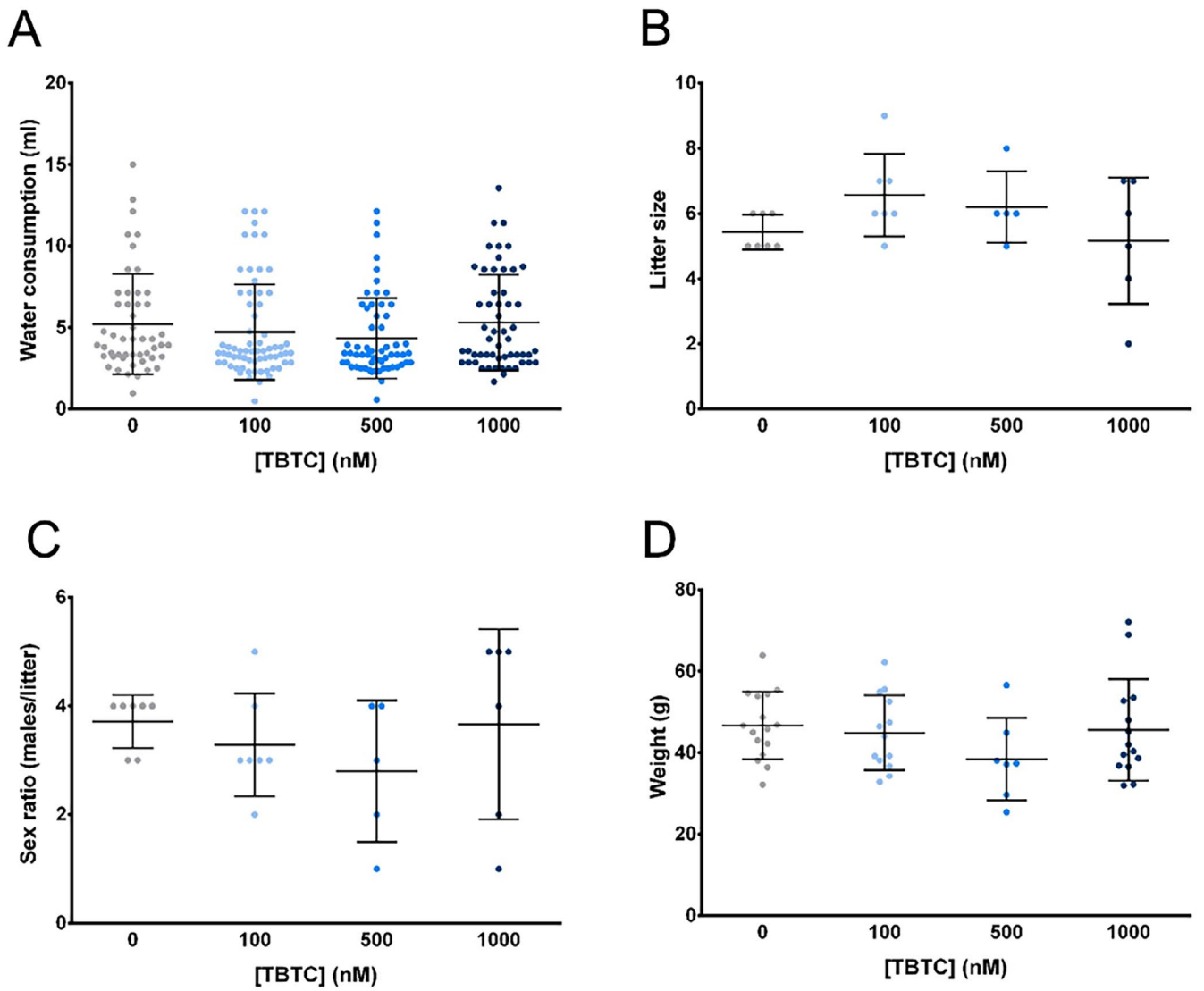

FIGURE 1 | Mouse parameters. (A) Water consumption (ml/day per mouse). (B) Litter size (pups per litter). (C) Sex ratio (males per litter). (D) Mouse weight (g).

doses [26]. Treatment was continued throughout gestation and lactation and ended upon weaning of the pups. The duration of exposure was 5 days before mating, plus 20 days of gestation and 21 days of lactation—that is, 46 days. Females were housed two per cage and drank the TBTC- or vehicle-containing water solutions ad libitum; fresh solutions were prepared and replaced every week after water intake was measured. Consumption was measured per bucket, determining the milliliters remaining when the bottle was changed. The average milliliters consumed per animal per day was calculated. There were no differences in water consumption between the groups (Figure 1A). The amount of TBTC ingested was 154, 708, and 1724 ng per mouse/day for the groups that drank water containing 100, 500, and 1000 nM, respectively. Some females were either not pregnant or did not deliver (whereas incidence was not dose-related), and a total of 21 litters were used for the remainder of the study. At birth, litter size (Figure 1B) and sex ratio (Figure 1C) were recorded.

Pups were weaned at day 21, males were housed in groups of 3–5 mice per cage. In male offsprings, locomotor activity and olfactory function were assessed at 15, 19, and 24 months of age. Each group consisted of at least 10 mice from at least five different litters. The sample size ranges 10–20. Although PD also affects females, we only studied male mice, because PD is an age-associated disease and females spend one third of their lives in menopause, a condition that does not occur in mice and complicates disease modeling [23]. At the end of the study, males were sacrificed by cervical dislocation without anesthesia and, after rapid decapitation, brains were removed. Each brain was bisected along the midline. One hemisphere was immediately frozen in liquid nitrogen and stored at −80°C until use. The other hemisphere was fixed in 4% paraformaldehyde.

2.3 | Genetic Analysis

Total DNA was extracted from the biological samples by conventional methods. As described previously, mtDNA deletions were detected and analyzed by long-range PCR [25]. mtDNA copy number was quantified by qPCR using a StepOne Real-Time PCR System as previously described [27]. Six

independently isolated samples were measured in duplicate. The mtDNA Control Region was amplified and sequenced according to protocols previously described [28]. PCR primers were hmtL15591: 5′-TTCGCCTACACAATTCTCCG-3′ and hmtH626: 5′-TTTATGGGGTGATGTGAGCC-3′ and sequencing primers were hmtL15591, hmtH626, and hmtL16365: 5′-GTCAAATCCCTTCTCGTCCC-3′. The revised Cambridge reference sequence (GenBank, NC_012920) was used to locate mutations.

Mice mtDNA deletions were detected and analyzed by long-range PCR with MsmtL293: 5′-TAAACGAAAGTTTGACTA AGTTATACCTCTTAGGG-3′ and MsmtH171: 5′-TTAAGC TATTTTAATGTGCTTGATACCCTCTCC-3′ primers. Mice mtDNA copy number was quantified by qPCR using a StepOne Real-Time PCR System. A mtDNA 12S ribosomal Custom Plus TaqMan RNA Assay (Applied Biosystems, Assay ID: AR7DT9P) was used. The TaqMan probe was labeled at the 5′ end with a fluorescent reporter, 6FAM. mtDNA quantity was corrected by simultaneous measurement of a single copy nuclear *RNaseP* gene. A commercial kit was used to quantify nDNA (Applied Biosystems, Assay ID: Mm99999915_g1), and the nDNA-specific fluorescent probe was labeled internally using VIC fluorescent dye. The 20 μL PCR reaction contains 1×TaqMan Universal PCR Master Mix (Applied Biosystems, 4304437), 1 μL of *Gapdh* TaqMan Gene Expression Assay and 1 μL of 12S Custom Plus TaqMan RNA Assay, and 10 ng of total DNA extract. PCR conditions were 2 min at 50°C and 10 min at 95°C, followed by 40 cycles of 15 s of denaturation at 95°C and 60 s of annealing/extension at 60°C. The mice mtDNA Control Region was amplified with MsmtL15198: 5′-AACACCCATTTATTATCATTGGCC-3′ and MsmtH177: 5′-TAAGCTATTTTAATGTGCTTGATAC C-3′ primers and sequenced with MsmtL15198, MsmtH177, and MsmtL15422: 5′-TGGTATTCTAATTAAACTACTTCTT G-3′ primers. GenBank DQ106412.1 was the mouse reference sequence.

2.4 | DNA Methylation Analysis

For quantitative determination of the percentage of whole genome 5-methylcytosine (5-mC) in mouse brain and cell culture derived samples, the MethylFlash Methylated DNA Quantification Kit (EpigenTek, P-1034-96) was used following the manufacturer's instructions.

2.5 | Gene Expression Analysis

For cultured cells, analysis of the expression of genes was performed by RT-qPCR using Cells-to Ct 1-Step TaqMan Kit (A25602) following the manufacturer's instructions. Cells were seeded and differentiated in 96-well format, culture media were removed, and cells were washed once with phosphate-buffered saline (PBS). Lysis solution containing DNase I was added, and the samples were incubated for 5 min at room temperature. Stop solution was added, and the samples were incubated for an additional 2 min at room temperature. The RT-qPCR reaction was carried out by adding 15 μL of the RT-qPCR master mix (containing TaqMan 1-Step qRT-PCR Mix, 20×-TaqMan Gene Expression Assay, and 20×-TaqMan Housekeeping Gene Expression) to a final 1× concentration and 5 μL of lysates. 20× TaqMan Assays were purchased from Thermo Fisher (*GAPDH*: Hs02786624_g1; *TUBB3*: Hs00801390_s1; *MAP2*: Hs00258900_m1; *TH*: Hs01002188_g1; *NRF1*: Hs00602161_m1). For mice experiments, total RNA was isolated from each mouse brain using a NucleoSpin RNA extraction Kit (Macherey-Nagel). Total RNA (1 μg) was reverse transcribed using the Transcriptor First Strand cDNA Synthesis Kit (Roche). Relative quantification of mRNA expression was performed by TaqMan real-time PCR using the commercial probes, according to the manufacturer's protocol [20]. Probes were as follows: *Gapdh*: Mm99999915_g1; *Ppargc1a*: Mm01208835_m1; *Tubb3*: Mm00727586_s1; *Map2*: Mm00485231_m1.

2.6 | Immunofluorescence

For fluorescent microscopy, cultured cells were fixed with 4% paraformaldehyde for 15 min at room temperature and permeabilized with 0.1% Triton X-100 for 10 min. After blocking for 30 min with 5% bovine serum albumin, cells were incubated for 1 h at room temperature or overnight at 4°C with primary antibodies against Tubulin β-3 (TUBB3) (1:500, ab18207, Abcam) or Kinesin-1 (KNS1) (1:250, MAB1614, Merck). Subsequently, cells were incubated with fluorescence-labeled secondary Alexa Fluor 594 or 488 (1:1000, A11008 and A11005, Invitrogen, respectively) at room temperature for 1 h, protected from light. Cells were briefly incubated with 1 μM DAPI for nuclear staining. Between incubations, samples were washed with PBS containing 0.1% Triton X-100. Pictures were acquired using a Floyd Cell imaging station (Life Technologies) [25].

2.7 | Biochemical Analysis

Analyses of oxygen consumption, ATP, and H_2O_2 levels were performed according to previously described protocols [28]. Determination of the MIMP was performed using the Mito-ID Membrane Potential Detection Kit (Enzo Life Sciences). TBTC was added during the oxygen consumption analysis, or 2 days before the ATP, MIMP, and H_2O_2 levels determination.

2.8 | Electron Microscopy

Ultrastructural analysis was performed following a previously described procedure [11]. Briefly, cells were seeded in Permanox chamber slides (Nunc), fixed with 2.5% glutaraldehyde for 2 h at 4°C, and maintained in phosphate buffer supplemented with 0.05% sodium azide. Post-fixation was carried out using 1% OsO_4 for 2 h. Cells were dehydrated in a graded series of ethanol dilutions up to absolute. The specimens were then passed through different mixtures of ethanol and araldite (3:1, 1:1, and 1:3), and embedded in pure araldite. After 3 days of polymerization at 70°C, ultrathin sections were cut and stained following a protocol previously published [29]. The sections were examined with a JEOL 1010 transmission electron microscope using a Gatan Bioscan camera and Digital Micrograph software.

2.9 | Histologic Studies

Brains were harvested for histological analysis. The tissues were fixed in 4% paraformaldehyde fix solution and embedded in paraffin. The paraffin-embedded tissues were sectioned into 4 mm-slices and stained with hematoxylin and eosin (H&E, Sigma). Immunohistochemical staining of TH (Cat. #: T8700, Sigma-Aldrich. Antibody dilution 1:100), NeuN (Cat. #: ab104224, Abcam. Antibody dilution 1:100), and GFAP (Cat. #: 3893, Sigma-Aldrich. Antibody dilution 1:100) were executed following the manufacturer's protocols for the PolyStain TS Kit—for 2 Mouse and 1 Rabbit antibody on Rodent tissue (DAB/Permanent Red/Ni-DAB) (Neo Biotech).

The Periodic Acid-Schiff and Luxol Fast Blue stainings were carried out with commercial kits (PAS Staining System: Cat. #: 395B, Sigma-Aldrich; LFB staining: Cat. #: ab150675, Abcam).

2.10 | Time-Lapse Imaging of Neuronal Differentiation

SH-SY5Y cells and hNSCs were plated in a six-well plate and set for neuronal differentiation with/without TBTC as previously described. The plate was imaged using an Incucyte SX5 Live-Cell Analysis System (Essen Bioscience, Ann Arbor, MI) every 12 h for 7 days. The growth rate in each well was obtained by measuring the surface area covered and expressed as Phase Area Confluence (%). Neurite length and branch points were quantified to evaluate neural network stability over time, expressed as mm/mm^2 and neurite branch points/mm^2, respectively. Analysis was performed using Incucyte's NeuroTrack software.

2.11 | Behavioral Analyses

Several tests, previously used for behavioral phenotyping of PD mouse models, were performed [30].

Open field test. Locomotor activity was evaluated using an open field test. Each mouse was placed in the center of the square arena (45 × 45 × 40 cm) and allowed to explore it for 15 min. Total distance (locomotor activity), movement time (in seconds), movement speed (cm/s), and center distance (the distance traveled in the center of the arena) were recorded using the computer-operated Smart Junior video tracking system (Panlab).

Hyposmia evaluation. To test the olfactory function, the cookie-finding test was performed. The mice were familiarized with the chocolate cookie for 3 days before the test. Food restriction was applied for over 18 h before the test. For testing, each mouse was placed individually into a clean cage containing 3 cm of fresh bedding and allowed to acclimate for 5 min. After acclimation, a chocolate cookie (3 g) was buried 0.5 cm under the bedding in one corner of the cage and the mouse was placed at the opposite edge. The latency for the mouse to uncover the cookie was measured up to a maximum parameter of 15 min, as previously described [31].

2.12 | Statistical Analysis

All statistical analyses were performed using GraphPad Prism version 8.0.1. Data are presented as mean ± standard deviation. Statistical significance between experimental groups was assessed using either parametric tests (ANOVA and Student's *t*-test) or nonparametric tests (Kruskal–Wallis and Mann–Whitney U tests), depending on whether the data followed a normal distribution. A p-value of < 0.05 was considered statistically significant. All samples were analyzed in at least three independent biological replicates.

3 | Results

3.1 | Effect of Tributyltin Chloride on Oxidative Phosphorylation Systems of Neurons or Neuron-Precursor Cells

3.1.1 | SH-SY5Y Cells

To define the range of non-lethal TBTC concentrations in this cell type that would allow us to analyze its effect on OXPHOS function, we measured cell proliferation with different TBTC concentrations and observed a defect in the proliferation with TBTC concentrations ≥ 200 nM (Figure 2A). Next, we addressed the effect of TBTC on OXPHOS capacity from undifferentiated cells by measuring oxygen consumption and ATP levels. Acute exposure to ≥ 10 nM TBTC concentrations caused a statistically significant reduction in basal oxygen consumption (Figure 2B). The statistically significant increase in uncoupled oxygen consumption observed after the addition of FCCP to cells inhibited by 100 nM TBTC confirmed that this inhibitor acts by blocking the CV proton channel, not the electron transport chain complexes (ETC) (Figure 2C). In addition, cellular ATP levels generated in the mitochondria were also reduced at TBTC concentrations ≥ 50 nM (Figure 2D).

To analyze how TBTC may affect OXPHOS function of cells more dependent on this energetic source, we measured oxygen consumption of neuron-like cells incubated with different TBTC concentrations. Similar to undifferentiated cells, we observed a statistically significant reduction in basal oxygen consumption with ≥ 20 nM TBTC concentrations (Figure 2E). Finally, to address other potential effects of TBTC beyond OXPHOS inhibition in these cells, we analyzed mitochondrial morphology using electron microscopy and mtDNA levels by RT-qPCR. Neuronal differentiation of these cells in the presence of 50 nM TBTC resulted in the appearance of morphologically abnormal mitochondria, swollen and with a reduced number of mitochondrial cristae (Figure 2F). TBTC at 100 nM did not modify the mtDNA copy number in undifferentiated cells but reduced it in differentiated cells (Figure 2G).

3.1.2 | hNSCs

Similar to our analysis using SH-SY5Y cells, we defined a range of non-lethal concentrations of TBTC in hNSCs by measuring cell proliferation at different TBTC concentrations. A consistent defect in the proliferation of these cells was found with TBTC

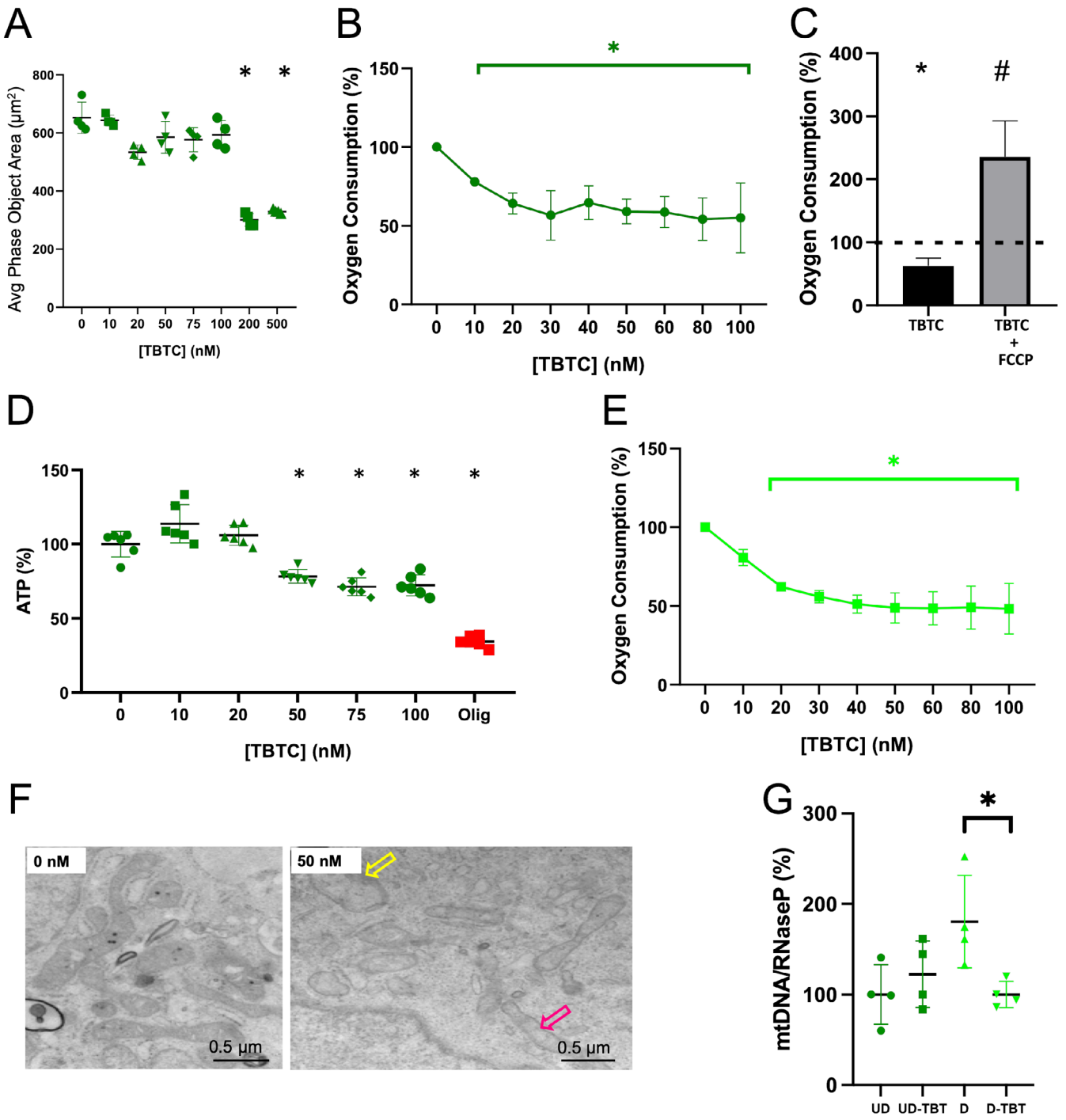

FIGURE 2 | Effect of tributyltin chloride (TBTC) on the oxidative phosphorylation system of human neuroblastoma cells SH-SY5Y. (A) Cell proliferation, determined as the average of the area of the objects in the image. $N = 4$. Kruskal–Wallis test. (B) Endogenous oxygen consumption in undifferentiated cells. $N = 3$. ANOVA. (C) Uncoupled oxygen consumption. TBTC (100 nM)- and TBTC (100 nM) + FCCP (100 nM)-treated cells. Dashed line shows the oxygen consumption in untreated undifferentiated cells. $N = 4$. Mann–Whitney test. (D) ATP levels in undifferentiated cells. Olig, codes for oligomycin, a complex V inhibitor, which was included as a positive control. $N = 6$. ANOVA. (E) Endogenous oxygen consumption in neuron-like cells. $N = 3$. ANOVA. (F) Electron microscopy images of neuron-like cells. Yellow and red arrows show abnormal mitochondria and lack of mitochondrial cristae, respectively. (G) Amount of mtDNA in undifferentiated (UD) and differentiated to neuron (D) cells. $N = 4$. Mann–Whitney test. Mean ± Standard Deviations are shown. * and # indicate statistically significant differences ($p < 0.05$) versus no-TBTC and TBTC no-FCCP, respectively.

concentrations ≥ 75 nM (Figure 3A). To address the effect of TBTC on OXPHOS capacity from these undifferentiated cells, we analyzed oxygen consumption and ATP levels. Acute exposure to ≥ 50 nM TBTC concentrations caused a statistically significant reduction in basal oxygen consumption (Figure 3B). In addition, cellular ATP levels generated in the mitochondria of these cells were also reduced at TBTC concentrations of 100 nM (Figure 3C).

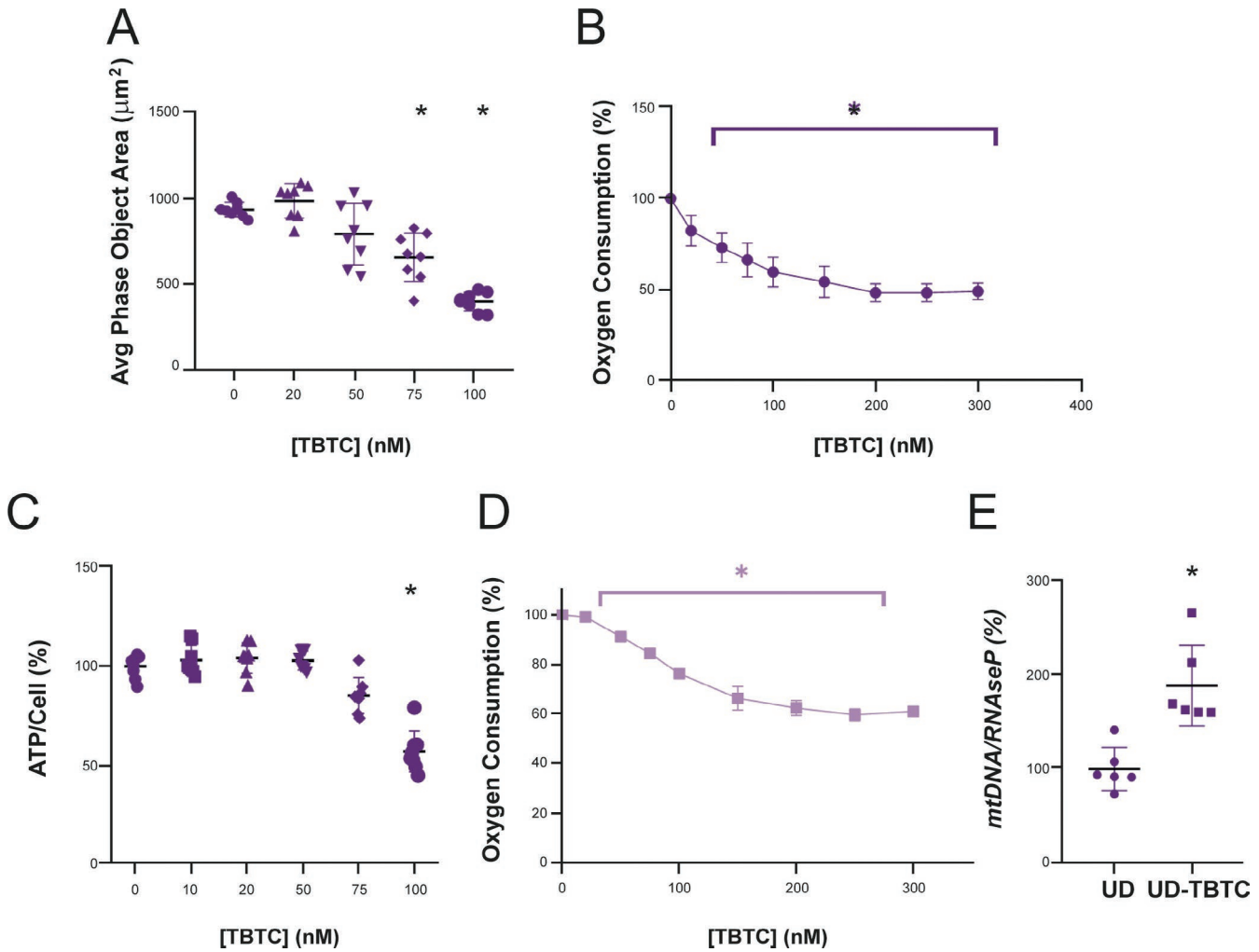

FIGURE 3 | Effect of tributyltin chloride (TBTC) on the oxidative phosphorylation system of human neural stem cells. (A) Cell proliferation, determined as the average of the area of the objects in the image. $N = 8$. Kruskal–Wallis test. (B) Endogenous oxygen consumption in undifferentiated cells. $N = 3$. ANOVA. (C) ATP levels in undifferentiated cells. $N = 8$. ANOVA. (D) Endogenous oxygen consumption in neuron-like cells. $N = 3$. ANOVA. (E) Amount of mtDNA in untreated and TBTC-treated undifferentiated (UD) cells. $N = 6$. Student's *t*-test. Mean ± Standard Deviations are shown. *, indicates statistically significant differences ($p < 0.05$) versus no-TBTC.

Next, we analyzed the OXPHOS inhibitory capacity in hNSCs derived neurons. There is a significant decrease in basal oxygen consumption when cells are exposed to ≥ 50 nM TBTC concentrations (Figure 3D).

Finally, to study the influence of TBTC on mitochondrial genome maintenance, we measured the mtDNA levels by RT-qPCR. Interestingly, 100 nM TBTC significantly increased the mtDNA copy number in undifferentiated cells (Figure 3E). Since neurons are highly dependent on OXPHOS function, neuronal differentiation is typically accompanied by an increase in mitochondrial biogenesis and mtDNA levels (Figure 2G). We have observed that TBTC impairs neuronal differentiation, which could account for the reduced mtDNA levels in differentiated cells exposed to TBTC (Figure 2G). Conversely, in undifferentiated, proliferative cells, TBTC exposure may trigger a compensatory response that leads to an increase in mtDNA levels. This effect is evident not only in hNSCs (Figure 3E) but also in undifferentiated SH-SY5Y cells (Figure 2G). Notably, such a compensatory response is absent in differentiated cells.

3.2 | Effect of Tributyltin Chloride on Neuronal Differentiation

3.2.1 | SH-SY5Y Cells

After confirming the effect of TBTC on the function of the OXPHOS system of different cell types with neuronal differentiation capacity, we aimed to address how exposure to this toxicant influences the neural differentiation process. For that purpose, we analyzed cellular morphology of SH-SY5Y cells derived neurons using optic microscopy. We observed that concentrations ≥ 20 nM TBTC caused alterations in the neuronal differentiation of these cells (Figure 4A). Indeed, these TBTC concentrations reduced the length of neurites (Figure 4B) and the branching points (Figure 4C). Finally, immunofluorescent staining with tubulin beta-3 chain (TUBB3) confirmed that ≥ 20 nM TBTC diminished neuronal differentiation (Figure 4D). Moreover, ≥ 75 nM TBTC decreased *TUBB3* and microtubule-associated protein 2 (*MAP2*) mRNA levels (Figure 4E,F).

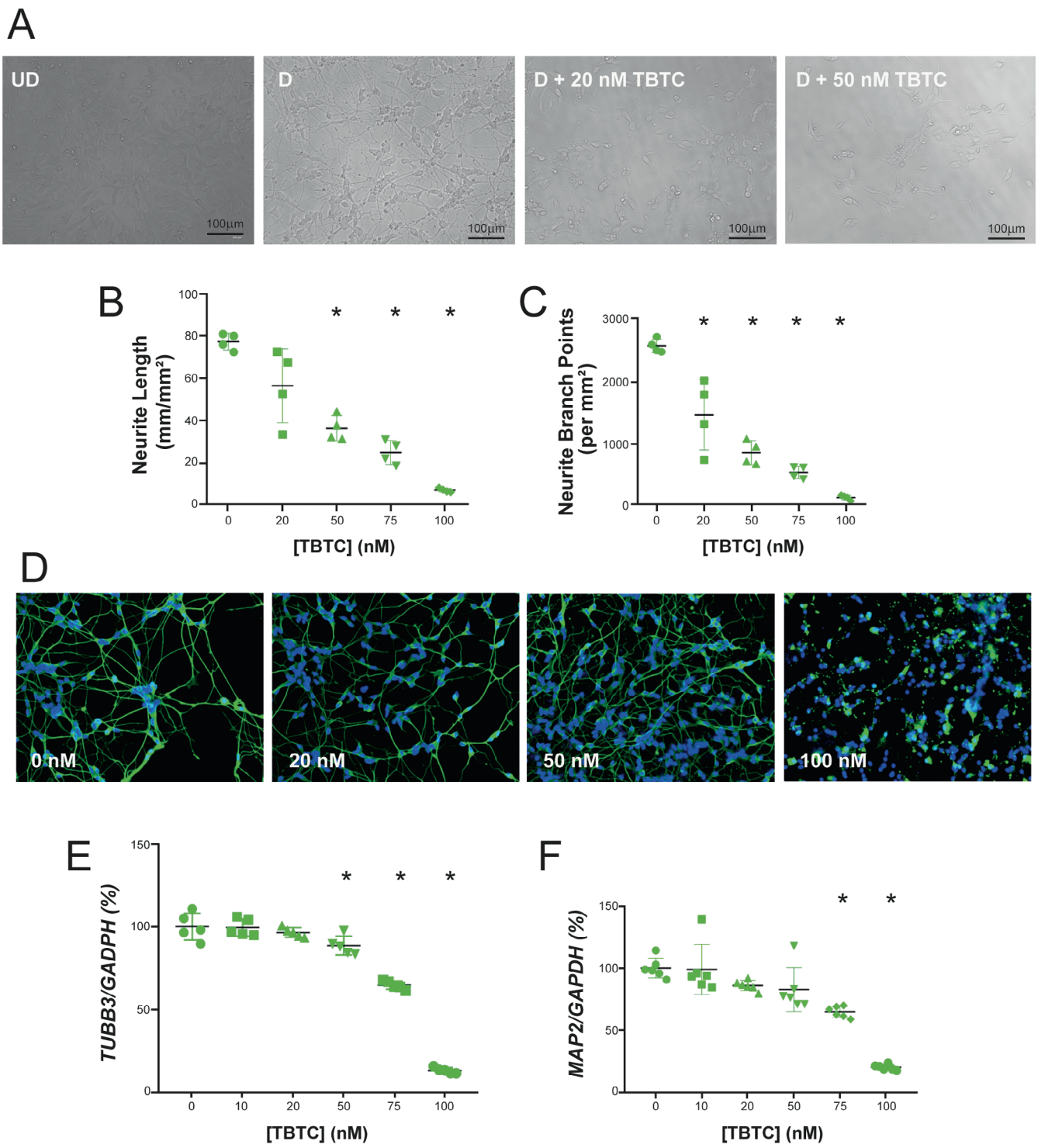

FIGURE 4 | Effect of tributyltin chloride (TBTC) on neuronal differentiation of human neuroblastoma cells SH-SY5Y. (A) Optic microscopy images showing undifferentiated (UD) and differentiated to neuron (D) SH-SY5Y cells. A reduction in the number and length of the neurites can be observed at different TBTC concentrations. (B) Neurite length. $N = 4$. Kruskal–Wallis test. (C) Neurite branching points. $N = 4$. Kruskal–Wallis test. (D) Immunofluorescence images of Tubulin beta-3 chain (green color). Nucleus are marked in blue color. (E) *TUBB3* mRNA levels. Glyceraldehide 3-phosphate dehydrogenase (*GAPDH*) mRNA was used to normalize. $N = 5$. Kruskal–Wallis test. (F) Microtubule associated protein 2 (*MAP2*) mRNA levels. *GAPDH* mRNA was used to normalize. $N = 6$. Kruskal–Wallis test. Mean ± Standard Deviations are shown. *, indicates statistically significant differences ($p < 0.05$) versus no-TBTC.

3.2.2 | hNSCs

Similar to the TBTC effects observed on SH-SY5Y cells, concentrations ≥ 20 nM TBTC cause alterations in neuronal differentiation of hNSCs, as can be observed by optic microscopy (Figure 5A). Remarkably, 100 nM TBTC reduces the length of neurites (Figure 5B) and the branching points (Figure 5C). TUBB3 immunofluorescence further demonstrated that ≥ 75 nM TBTC

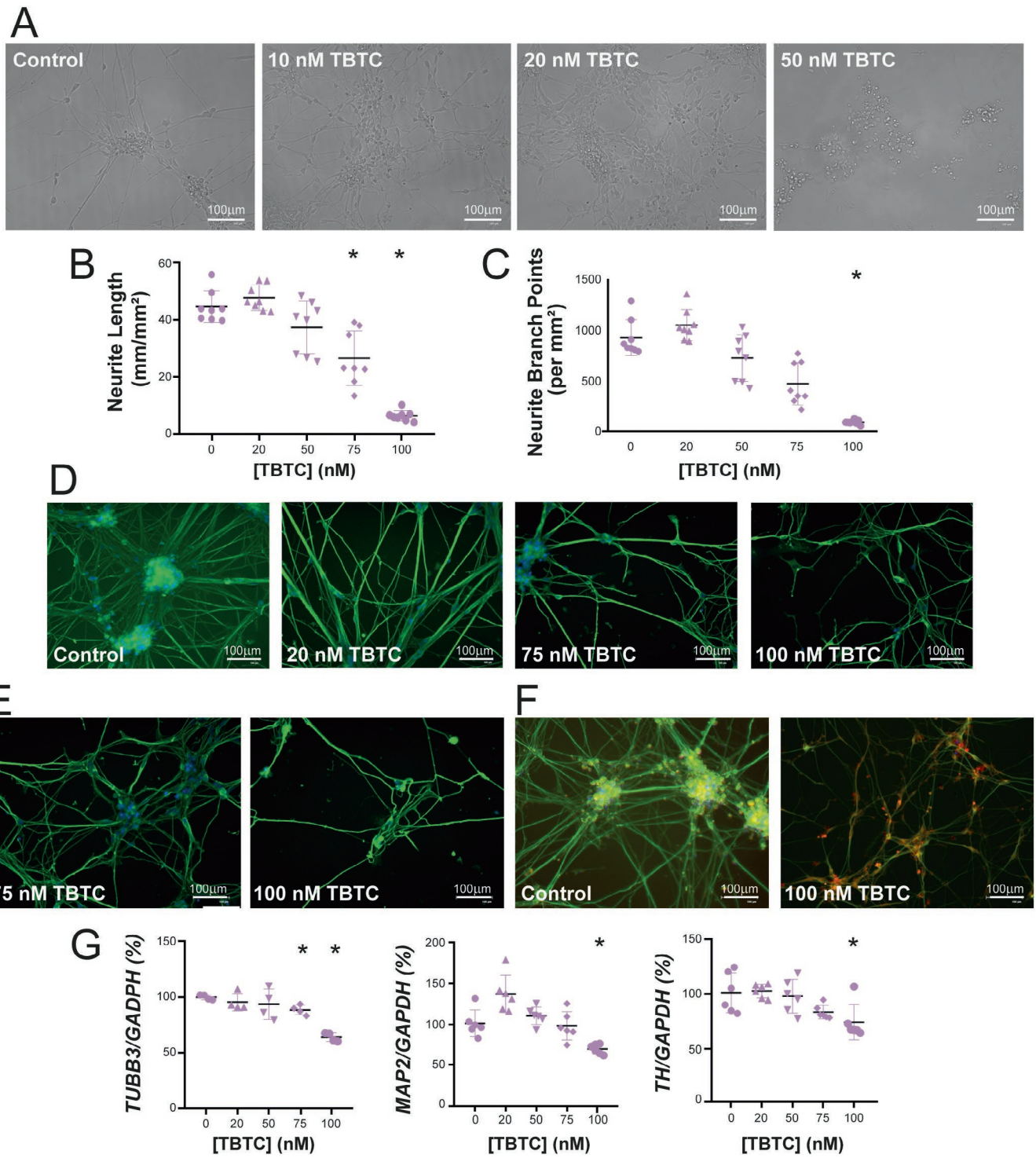

FIGURE 5 | Effect of tributyltin chloride (TBTC) on neuronal differentiation of human neural stem cells (hNSCs). (A) Optic microscopy images showing hNSCs-derived neurons. A reduction in the number and length of the neurites can be observed at different TBTC concentrations. (B) Neurite length. $N = 4$. Kruskal–Wallis test. (C) Neurite branching points. $N = 4$. Kruskal–Wallis test. (D) Immunofluorescence images of Tubulin beta-3 chain (*TUBB3*), green color, in hNSCs differentiated to neurons and treated with TBTC. (E) Immunofluorescence images of TUBB3 in differentiated hNSCs in the presence of TBTC. Pink and white arrows indicate neuritic beads and curved neurites, respectively. (F) Immunofluorescence images of TUBB3 and kinesin (red color) in differentiated hNSCs in the presence of TBTC. (G) *TUBB3*, Microtubule associated protein 2 (*MAP2*), and Tyrosine hydroxylase (*TH*) mRNA levels. Glyceraldehide 3-phosphate dehydrogenase (*GAPDH*) mRNA was used to normalize. ANOVA. Mean ± Standard Deviations are shown. *, indicates statistically significant differences ($p < 0.05$) versus no-TBTC.

diminished neuronal differentiation (Figure 5D). Thus, neurons derived from cells exposed to TBTC showed thinner neurites than control neurons, and neuritic beading, bead-like structures along the neurites which occur upon intracellular ATP decrease, were more commonly found in treated cells. In addition, "undecided," curved neurites were also more frequently found upon TBTC

exposure (Figure 5E). Interestingly, neuritic beads colocalized with kinesin, a motor protein involved in antegrade fast axonal transport (Figure 5F). Moreover, 100 nM TBTC affected expression of critical genes required for neuronal function, observed by decreased *TUBB3*, *MAP2*, and *TH* mRNA levels (Figure 5G).

3.3 | Genome Effect of Tributyltin Chloride

Several studies have shown that some organotins can be mutagenic [32]. Sequence analysis of the mtDNA non-coding control region of hNSCs and SH-SY5Y cells revealed six (m.200A > G, m.263A > G, m.309-310insC, m.315-316insC, m.16129G > A, m.16519 T > C) and four (m.263A > G, m.309-310insCCC, m.315-316insC, m.16519 T > C) genetic variants, respectively, when compared to the revised Cambridge Reference Sequence (rCRS). However, these variants, and no more, were also found in 100 nM TBTC-treated cells. Moreover, large deletions in the mtDNA were neither observed in these TBTC-treated cells (Figure 6A).

To address if this toxicant was able to modulate epigenetic reprogramming in these cell types, we analyzed whole genome epigenetic markers. TBTC-exposed SH-SY5Y cells showed a reduction in global DNA methylation levels, while this modification was increased in treated hNSCs (Figure 6B).

3.4 | Effect of Early Exposure to Tributyltin Chloride on Old Mice

To study the toxic effects of TBTC during early development in the context of a complete organism, we moved to a murine model. We treated mice with different TBTC regimes throughout gestation and lactation and measured the levels of mtDNA, its integrity and whole epigenetic markers. We did not find any reduction in mtDNA copy number, any accumulation of point mutations in the non-coding region of mtDNA, nor large mtDNA deletions in the brain of 24-month-old mice (Figure 7A,B). However, we observed a decrease of global DNA methylation following treatment with 1000 nM TBTC (Figure 7C).

In addition, we analyzed gene expression of some genes involved in OXPHOS function (*Pgc1a*, *Mt-rnr1*, *Mt-nd2*, *Mt-nd5*, *Mt-co1*, *Mt-atp6*) or neuronal differentiation (*Map2*, *TUBB3)* and found that in the brain of 24-month-old mice exposed to TBTC the mRNA levels of these genes were not reduced from control mice (Figure 7D).

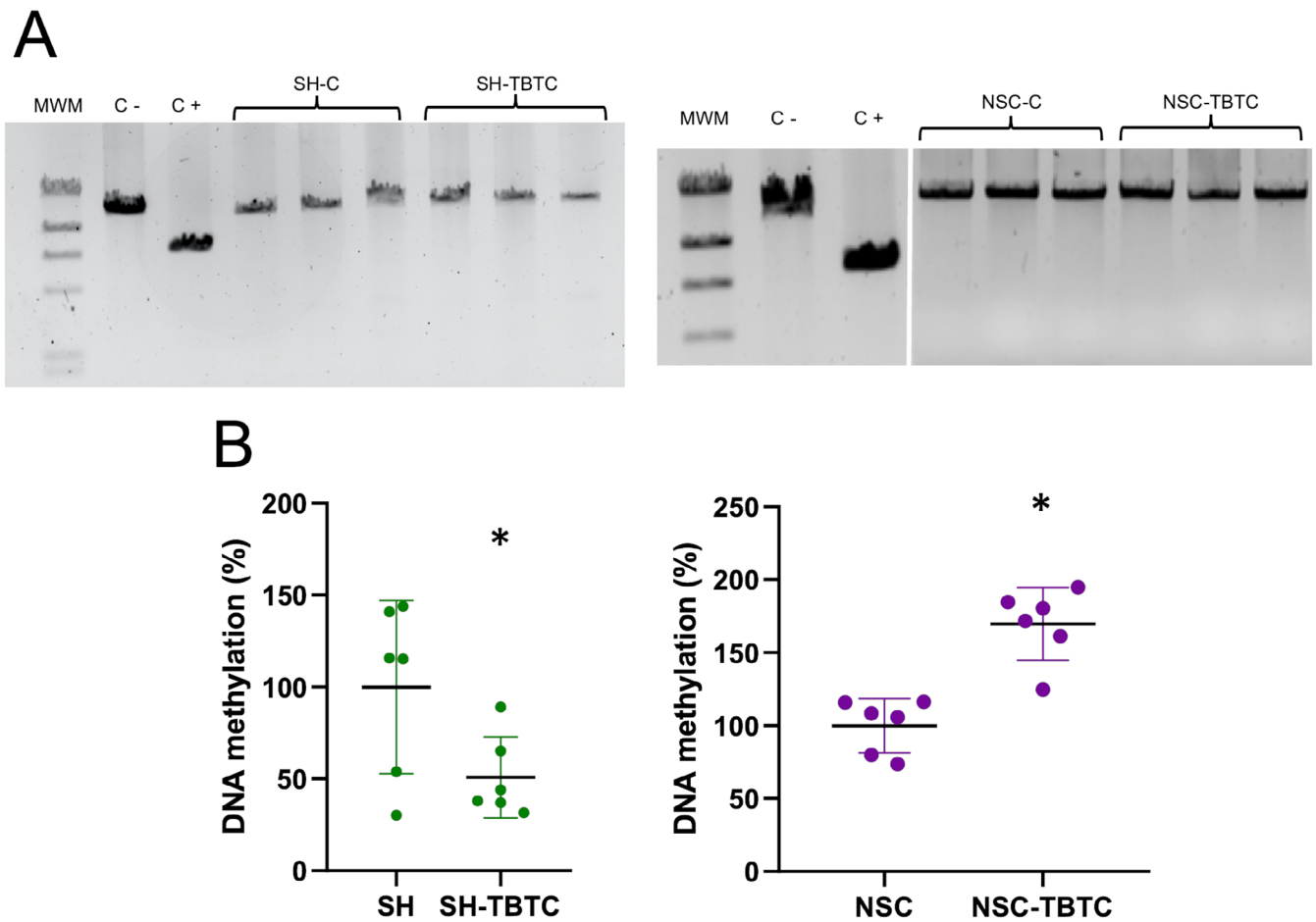

FIGURE 6 | Genomic effects of tributyltin chloride (TBTC) in undifferentiated cells. (A) Large deletions in the mtDNA. MWM, molecular weight marker; C-, negative control; C+, positive control; SH-C, untreated SH-SY5Y cells; SH-TBTC, TBTC-treated SH-SY5Y cells; NSC-C, untreated neural stem cells; NSC-TBTC, TBTC-treated NSC. The second image is a composite of two gels run with samples amplified simultaneously. (B) Global DNA methylation. $N = 6$. Mean ± Standard Deviations are shown. *, indicates statistically significant differences ($p < 0.05$) versus no-TBTC.

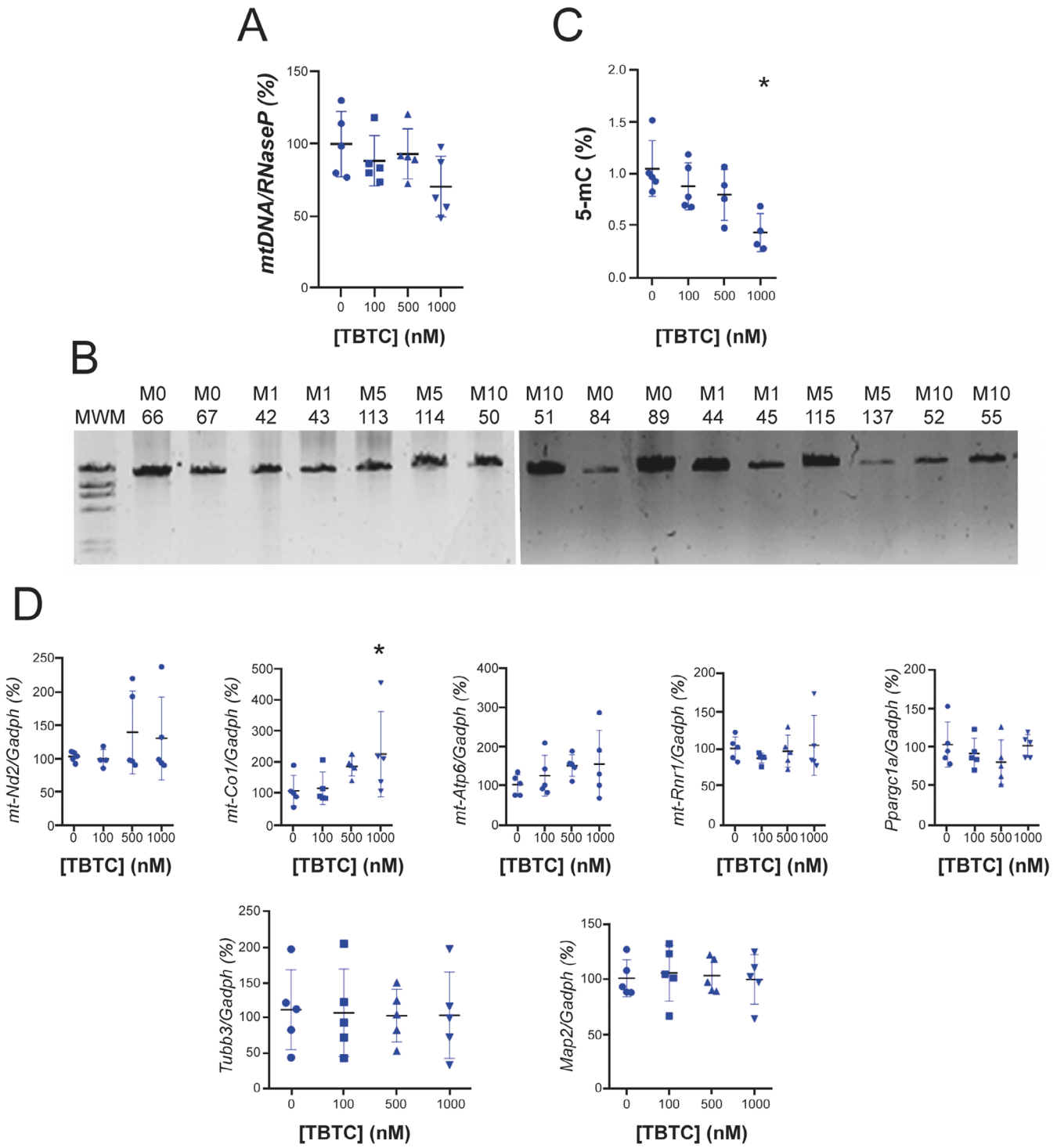

FIGURE 7 | Effect of early exposure to tributyltin chloride (TBTC) in old mice brains. (A) mtDNA copy number. *RNaseP* gene was used to normalize. $N = 5$. (B) Large mtDNA deletions. This test was only performed on mice exposed to 1000 nM of TBTC. MWM, molecular weight marker. Student's *t*-test. The image is a composite of two gels run with samples amplified simultaneously. (C) Global DNA methylation. $N = 5$. (D) mRNA levels of mitochondria-related and neuronal differentiation-related transcripts. *Gapdh* mRNA was used to normalize. $N = 5$. Mean ± Standard Deviations are shown. *, indicates statistically significant differences ($p < 0.05$) versus no-TBTC.

To address if TBTC has any impact in the physiological function of these mice, we performed behavioral analyses. Total distance and mean speed of 19- and 24-month-old mice were significantly lower than those of 15-month-old mice (Figure 8A,B), a result that was previously shown [33]. Moreover, the time elapsed to find the cookie was significantly lower in 15-month-old mice than older mice (Figure 8C). However, there were no differences among these parameters upon TBTC treatment at different concentrations (Figure 8A–C).

There were no differences in weights at the time of slaughter (Figure 1D), but interestingly, although they could not be

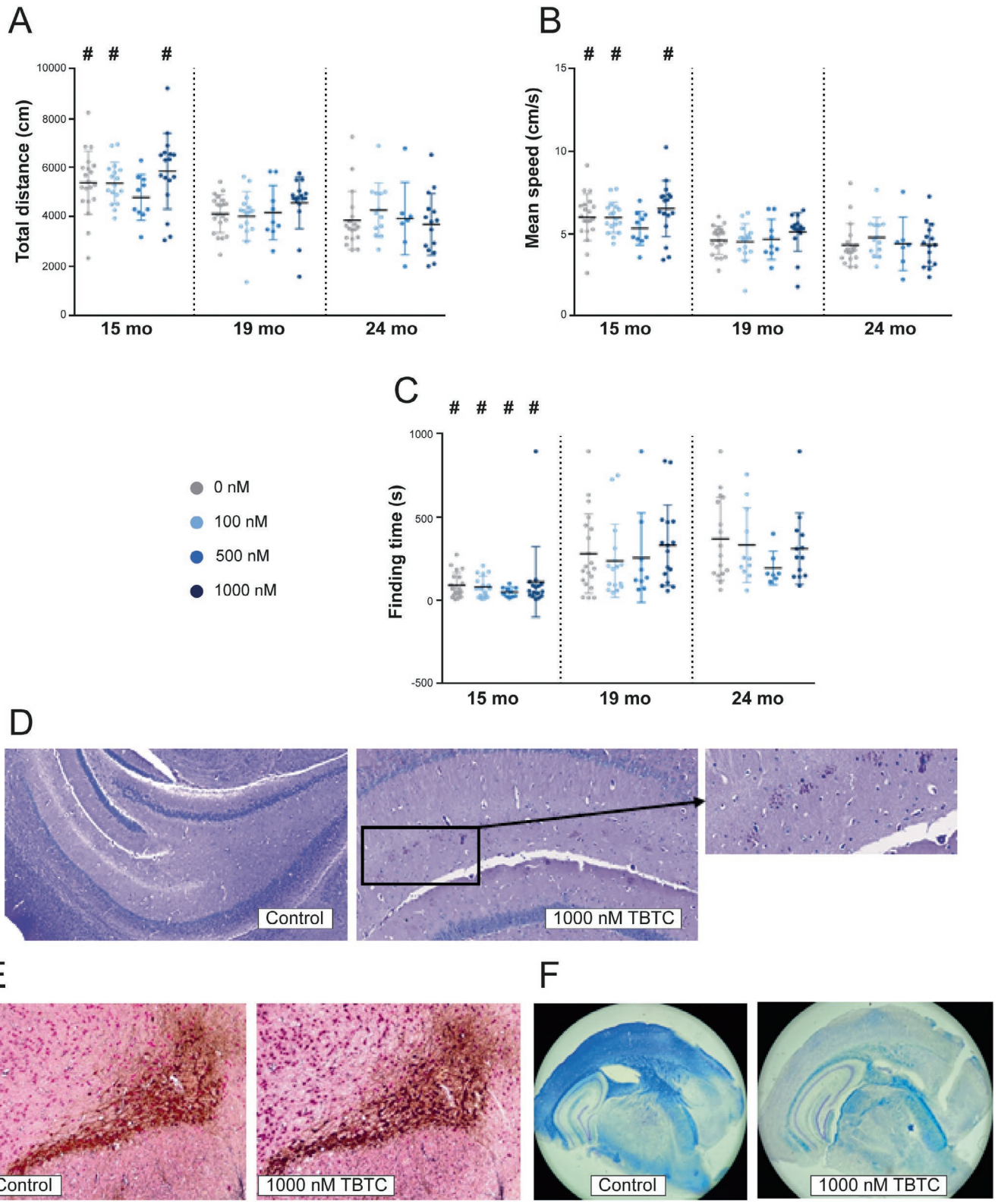

FIGURE 8 | Effect of early exposure to tributyltin chloride (TBTC) on functional tests and brain anatomopathology of old mice. (A–C) Total distance, mean speed, and cookie finding test in untreated and TBTC-treated mice of different ages. Mean ± Standard Deviations are shown. #, indicates statistically significant differences ($p < 0.05$) versus older mice. Kruskal–Wallis test. (D) Periodic acid-Schiff (PAS) granules in hippocampus from aged mice. (E) Astrocytosis in hippocampus from aged mice. (F) Demyelination from hippocampus from aged mice.

quantified, some histological alterations were observed in the brains of these mice. Thus, the hippocampus of aged mice treated in utero and during lactation with 1000 nM TBTC showed an abundance of periodic acid-Schiff (PAS) granules (Figure 8D), *substantia nigra* showed astrocytosis (Figure 8E), and there was general demyelination (Figure 8F).

4 | Discussion

It has been demonstrated that TBTC is neurotoxic in vitro at levels detected in human blood samples. This result suggests the possibility that chronic exposure to low levels of TBTC in humans during the development of the nervous system may be neurotoxic and promote the onset of neurodegenerative diseases in late life.

Previous results from our group showed that TBTC affects OXPHOS function of several cell types [11, 12]. We now extend these observations to neurons and neuron precursor cells. To compromise the viability and proliferation of hNSCs, SH-SY5Y, or other cells, depending on the duration of treatment, TBT concentrations equal to or higher than 75 nM are required [34]. Our results show that 50 nM TBTC causes the appearance of morphologically abnormal mitochondria in neuron-differentiated SH-SY5Y cells. Swollen mitochondria with fewer cristae have already been described in other TBTC-exposed cells [35]. Moreover, we showed that ≥ 20 nM TBTC is harmful to the OXPHOS function of neuronal precursor cells. This is consistent with previous results showing that MIMP was diminished in SH-SY5Y cells treated with 300 nM TBTC [36], and that ATP levels and MIMP were decreased in hiPSCs treated with 50 nM TBT [37]. It was also reported that TBTC caused a significant decrease in MIMP in dissociated mixed cells from different parts of the rat brain, being striatum cells the ones showing the higher susceptibility [38]. Fetal rat primary cortical neurons exposed to 20 nM TBTC showed decreased expression of some OXPHOS subunits mRNAs and reduced ATP content [39]. In addition, TBT 200 nM decreased ATP levels and MIMP in mouse sensory dorsal root ganglion neurons and, similar to our results, provoked neuritic beading [40]. Interestingly, like TBTC, which binds to the ATP6 subunit and inhibits CV, the m.8993 T > G mutation affecting the ATP6 subunit of CV encoded by mtDNA and a depletion of the alpha subunit of CV encoded by nDNA all cause neuritic beading [41]. The neuritic beading is also associated with other conditions that reduce ATP levels [42], and it has been frequently associated with mitochondrial abnormalities [43].

Our results show that TBTC is harmful to neuronal differentiation. This is consistent with a significantly reduced gene expression of ectodermal marker *OTX2* that regulates neurogenesis in hiPSCs treated with 50 nM TBT [44]. TBT exposure also significantly decreased the percentage of PAX6 positive cells, a marker of neuroectoderm, and downregulated the expression of Nestin, a marker of neuronal progenitor cells [44]. These data suggest that TBT can induce developmental neurotoxicity via mitochondrial dysfunction. Interestingly, low-dose TBT also significantly inhibited myogenic differentiation [45], but promoted adipocyte differentiation [11]. Although TBTC has the greatest effect on cells that are differentiating into neurons, it also negatively affects fully differentiated neurons. TBTC exposure reduced the number of neurons in primary cultures from the cerebral cortex of fetal rats [46]. TBT caused extensive axon degeneration in mouse sensory dorsal root ganglion neurons [40]. In addition, neurons were shown to be more vulnerable to TBT than other brain cells [47].

If early exposure to TBTC during nervous system development affects neuronal proliferation and differentiation and increases the risk of age-associated diseases, such as PD, it is plausible that permanent cellular modifications may occur. The TBTC exposure does not increase the frequency of mtDNA mutations, but it does cause a different effect on the global DNA methylation levels of hNSCs and SH-SY5Y cells. Both no effect and hypomethylation have been observed in cells exposed to TBT [48]. However, more detailed analyses have shown that some genes may be hypomethylated and others hypermethylated [36]. Modification of gene methylation patterns could be a signal that is perpetuated over time and links early TBTC exposure to very late-life effects.

Treatment with TBTC in utero and during lactation reduces global DNA methylation levels in the brains of 24-month-old male mice. However, we found no other quantitative differences in either OXPHOS function, neuronal differentiation, or motor and olfactory behavior between TBTC-exposed and non-exposed mice. On postnatal day (PND) 20, MAP2 immunostaining of cerebral cortex and hippocampal CA3 of mice prenatally exposed to TBT was not different from that of unexposed mice [39]. Furthermore, no significant differences in movement speed or distance in the open field test were found in PND25 male rats perinatally exposed to TBTC compared to non-exposed ones [49]. On the other hand, administration of TBT to postnatal mice caused a decrease in locomotion activity [50]. In addition, TBT decreased tyrosine hydroxylase (*TH*) mRNA levels, its activity, and dopamine content in rat pheochromocytoma PC12 cells [51]. TH is the rate-limiting enzyme in dopamine synthesis, and this is the main neurotransmitter affected in PD. TBT decreased *TH* mRNA levels in zebrafish brain [52] and dopamine levels in the brain of male medaka [53]. It also reduced dopamine levels in rat brain, eliciting neurodegenerative changes [54]. The exposure to TBTC resulted in a decrease in cell viability in various parts of the rat brain, with the striatum showing the greatest vulnerability at a concentration of 30 nM [55]. Moreover, a single acute exposure to TBTC decreased rat spontaneous motor activity [56]. Therefore, it can be concluded that exposure to TBT is toxic to the nervous system [57].

Despite the variables that we have quantified in mice exhibiting no significant differences compared to the control group, other parameters could be modified in the brains of these mice. In this regard, we have noted some histopathologic changes, such as demyelination and astrocytosis. Differentiation of oligodendrocyte precursor cells (OPCs), and therefore axonal myelination, is very sensitive to sublethal mitochondrial dysfunction [58]. Cuprizone, as TBTC, alters OXPHOS function in the central nervous system of mice. In the cuprizone-based model of demyelination, astrocytes become hypertrophic and hyperplastic before myelin loss [59]. Acute administration of TBT to the neonatal rat caused decrements in myelin basic protein, an indicator for myelinogenesis [57]. TBT produces astrocyte stellation and activation [38].

Exposure to certain pesticides has been associated with an increased risk of developing PD. For instance, developmental exposure to dieldrin induces epigenetic alterations in genes involved in the development and maintenance of dopaminergic neurons. These epigenetic modifications persist beyond the exposure period and disrupt critical neurodevelopmental pathways, potentially increasing the risk of neurodegenerative diseases later in life, such as PD [60]. Developmental effects of xenobiotics are a matter of concern, because they are often induced by doses considerably lower than the one considered safe for adults and persist throughout life [61]. Highly lipophilic organotin compounds readily cross the blood–brain barrier with striatal cells showing greater susceptibility than

those from other brain regions [62, 63]. In a previous work, we indicated that high TBTC concentrations might provoke severe diseases in childhood, such as striatal necrosis syndromes [12]. Now, we suggest that exposure to low TBT concentrations during perinatal life may have effects on neuronal differentiation and brain development that could be critical for the onset of disease in adulthood, such as Parkinson disease, another disease affecting striatum.

Author Contributions

E.L.-G. and E.R.-P. contributed to the study conception and design. Material preparation, data collection and analysis were performed by all authors. The first draft of the manuscript was written by E.R.-P. and all authors commented on previous versions of the manuscript. All authors read and approved the final manuscript.

Acknowledgments

We would like to thank Santiago Morales for his assistance with figures.

Funding

This work was supported by grants from Instituto de Salud Carlos III (ISCIII-FIS-PI21/00229) and European Regional Development Fund (FEDER); Ministerio de Ciencia e Innovación [PID2023-147275NB-I00, PID2024-159386OA-I00 and CNS2023-144637]; Gobierno de Aragón (Grupos Consolidados B33_23R); and Fundación Mutua Madrileña (MMA). CIBERER is an initiative of the ISCIII.

Conflicts of Interest

The authors declare no conflicts of interest.

Data Availability Statement

The data that support the findings of this study are available from the corresponding author upon reasonable request.

References

1. F. Grün, "The Obesogen Tributyltin," *Vitamins and Hormones* 94 (2014): 277–325.

2. M. M. Whalen, B. G. Loganathan, and K. Kannan, "Immunotoxicity of Environmentally Relevant Concentrations of Butyltins on Human Natural Killer Cells In Vitro," *Environmental Research* 81 (1999): 108–116, https://doi.org/10.1006/enrs.1999.3968.

3. J. Beyer, Y. Song, K. E. Tollefsen, et al., "The Ecotoxicology of Marine Tributyltin (TBT) Hotspots: A Review," *Marine Environmental Research* 179 (2022): 105689, https://doi.org/10.1016/j.marenvres.2022.105689.

4. R. G. Uc-Peraza, Í. B. Castro, and G. Fillmann, "An Absurd Scenario in 2021: Banned TBT-Based Antifouling Products Still Available on the Market," *Science of the Total Environment* 805 (2022): 150377, https://doi.org/10.1016/j.scitotenv.2021.150377.

5. C. von Ballmoos, J. Brunner, and P. Dimroth, "The Ion Channel of F-ATP Synthase Is the Target of Toxic Organotin Compounds," *Proceedings of the National Academy of Sciences* 101 (2004): 11239–11244, https://doi.org/10.1073/pnas.0402869101.

6. W. N. Aldridge, "The Biochemistry of Organotin Compounds. Trialkyltins and Oxidative Phosphorylation," *Biochemical Journal* 69 (1958): 367–376, https://doi.org/10.1042/bj0690367.

7. A. P. Dawson and M. J. Selwyn, "The Action of Tributyltin on Energy Coupling in Coupling-Factor-Deficient Submitochondrial Particles," *Biochemical Journal* 152 (1975): 333–339, https://doi.org/10.1042/bj1520333.

8. S. Nesci, V. Ventrella, F. Trombetti, M. Pirini, A. R. Borgatti, and A. Pagliarani, "Tributyltin (TBT) and Dibutyltin (DBT) Differently Inhibit the Mitochondrial Mg-ATPase Activity in Mussel Digestive Gland," *Toxicology In Vitro* 25 (2011): 117–124, https://doi.org/10.1016/j.tiv.2010.10.001.

9. S. Nesci, V. Ventrella, F. Trombetti, M. Pirini, and A. Pagliarani, "Tributyltin (TBT) and Mitochondrial Respiration in Mussel Digestive Gland," *Toxicology In Vitro* 25 (2011): 951–959, https://doi.org/10.1016/j.tiv.2011.03.004.

10. S. Ueno, "Effects of Butyltin Compounds on Mitochondrial Respiration and Its Relation to Hepatotoxicity in Mice and Guinea Pigs," *Toxicological Sciences* 75 (2003): 201–207, https://doi.org/10.1093/toxsci/kfg153.

11. L. Llobet, J. M. Toivonen, J. Montoya, E. Ruiz-Pesini, and E. López-Gallardo, "Xenobiotics That Affect Oxidative Phosphorylation Alter Differentiation of Human Adipose-Derived Stem Cells at Concentrations That Are Found in Human Blood," *Disease Models & Mechanisms* 8 (2015): 1441–1455, https://doi.org/10.1242/dmm.021774.

12. E. López-Gallardo, L. Llobet, S. Emperador, J. Montoya, and E. Ruiz-Pesini, "Effects of Tributyltin Chloride on Cybrids With or Without an ATP Synthase Pathologic Mutation," *Environmental Health Perspectives* 124 (2016): 1399–1405, https://doi.org/10.1289/EHP182.

13. F. D. Dudimah, S. O. Odman-Ghazi, F. Hatcher, and M. M. Whalen, "Effect of Tributyltin (TBT) on ATP Levels in Human Natural Killer (NK) Cells: Relationship to TBT-Induced Decreases in NK Function," *Journal of Applied Toxicology* 27 (2007): 86–94, https://doi.org/10.1002/jat.1202.

14. N. J. Snoeij, P. M. Punt, A. H. Penninks, and W. Seinen, "Effects of Tri-n-Butyltin Chloride on Energy Metabolism, Macromolecular Synthesis, Precursor Uptake and Cyclic AMP Production in Isolated Rat Thymocytes," *Biochimica et Biophysica Acta—Bioenergetics* 852 (1986): 234–243, https://doi.org/10.1016/0005-2728(86)90228-8.

15. S. Yamada, Y. Kotake, Y. Demizu, et al., "NAD-Dependent Isocitrate Dehydrogenase as a Novel Target of Tributyltin in Human Embryonic Carcinoma Cells," *Scientific Reports* 4 (2015): 5952, https://doi.org/10.1038/srep05952.

16. X. Yan, B. He, L. Liu, et al., "Organotin Exposure Stimulates Steroidogenesis in H295R Cell via cAMP Pathway," *Ecotoxicology and Environmental Safety* 156 (2018): 148–153, https://doi.org/10.1016/j.ecoenv.2018.03.028.

17. B. W. Daigneault and J. D. de Agostini Losano, "Tributyltin Chloride Exposure to Post-Ejaculatory Sperm Reduces Motility, Mitochondrial Function and Subsequent Embryo Development," *Reproduction, Fertility, and Development* 34 (2022): 833–843, https://doi.org/10.1071/RD21371.

18. C. L. V. Pereira, C. F. Ximenes, E. Merlo, et al., "Cardiotoxicity of Environmental Contaminant Tributyltin Involves Myocyte Oxidative Stress and Abnormal Ca^{2+} Handling," *Environmental Pollution* 247 (2019): 371–382, https://doi.org/10.1016/j.envpol.2019.01.053.

19. N. Sharma and A. Kumar, "Mechanism of Immunotoxicological Effects of Tributyltin Chloride on Murine Thymocytes," *Cell Biology and Toxicology* 30 (2014): 101–112, https://doi.org/10.1007/s10565-014-9272-7.

20. E. Iglesias, M. P. Bayona-Bafaluy, A. Pesini, et al., "Uridine Prevents Negative Effects of OXPHOS Xenobiotics on Dopaminergic Neuronal Differentiation," *Cells* 8 (2019): 1407, https://doi.org/10.3390/cells8111407.

21. E. Iglesias, A. Pesini, N. Garrido-Pérez, et al., "Prenatal Exposure to Oxidative Phosphorylation Xenobiotics and Late-Onset Parkinson Disease," *Ageing Research Reviews* 45 (2018): 24–32, https://doi.org/10.1016/j.arr.2018.04.006.

22. A. Pesini, E. Iglesias, M. P. Bayona-Bafaluy, et al., "Brain Pyrimidine Nucleotide Synthesis and Alzheimer Disease," *Aging* 11 (2019): 8433–8462, https://doi.org/10.18632/aging.102328.

23. I. Jiménez-Salvador, P. Meade, E. Iglesias, P. Bayona-Bafaluy, and E. Ruiz-Pesini, "Developmental Origins of Parkinson Disease: Improving the Rodent Models," *Ageing Research Reviews* 86 (2023): 101880, https://doi.org/10.1016/j.arr.2023.101880.

24. K. U. S. Islam, N. Meli, and S. Blaess, "The Development of the Mesoprefrontal Dopaminergic System in Health and Disease," *Frontiers in Neural Circuits* 15 (2021): 746582, https://doi.org/10.3389/fncir.2021.746582.

25. C. Hernández-Ainsa, E. López-Gallardo, M. C. García-Jiménez, et al., "Development and Characterization of Cell Models Harbouring mtDNA Deletions for In Vitro Study of Pearson Syndrome," *Disease Models & Mechanisms* 15 (2022): dmm049083, https://doi.org/10.1242/dmm.049083.

26. M. Penza, M. Jeremic, E. Marrazzo, et al., "The Environmental Chemical Tributyltin Chloride (TBT) Shows Both Estrogenic and Adipogenic Activities in Mice Which Might Depend on the Exposure Dose," *Toxicology and Applied Pharmacology* 255 (2011): 65–75, https://doi.org/10.1016/j.taap.2011.05.017.

27. A. L. Andreu, R. Martinez, R. Marti, and E. García-Arumí, "Quantification of Mitochondrial DNA Copy Number: Pre-Analytical Factors," *Mitochondrion* 9 (2009): 242–246, https://doi.org/10.1016/j.mito.2009.02.006.

28. A. Gómez-Durán, D. Pacheu-Grau, E. López-Gallardo, et al., "Unmasking the Causes of Multifactorial Disorders: OXPHOS Differences Between Mitochondrial Haplogroups," *Human Molecular Genetics* 19 (2010): 3343–3353, https://doi.org/10.1093/hmg/ddq246.

29. E. S. Reynolds, "THE USE OF LEAD CITRATE AT HIGH pH AS AN ELECTRON-OPAQUE STAIN IN ELECTRON MICROSCOPY," *Journal of Cell Biology* 17 (1963): 208–212, https://doi.org/10.1083/jcb.17.1.208.

30. T. N. Taylor, J. G. Greene, and G. W. Miller, "Behavioral Phenotyping of Mouse Models of Parkinson's Disease," *Behavioural Brain Research* 211 (2010): 1–10, https://doi.org/10.1016/j.bbr.2010.03.004.

31. M. Yang and J. N. Crawley, "Simple Behavioral Assessment of Mouse Olfaction," *Current Protocols in Neuroscience* 48 (2009): 8.24.1–8.24.12, https://doi.org/10.1002/0471142301.ns0824s48.

32. J. Westendorf, H. Marquardt, and H. Marquardt, "DNA Interaction and Mutagenicity of the Plastic Stabilizer Di-n-Octyltin Dichloride," *Arzneimittel-Forschung* 36 (1986): 1263–1264.

33. S. Yanai and S. Endo, "Functional Aging in Male C57BL/6J Mice Across the Life-Span: A Systematic Behavioral Analysis of Motor, Emotional, and Memory Function to Define an Aging Phenotype," *Frontiers in Aging Neuroscience* 13 (2021): 697621, https://doi.org/10.3389/fnagi.2021.697621.

34. S. Hatamiya, M. Miyara, and Y. Kotake, "Tributyltin Inhibits Autophagy by Decreasing Lysosomal Acidity in SH-SY5Y Cells," *Biochemical and Biophysical Research Communications* 592 (2022): 31–37, https://doi.org/10.1016/j.bbrc.2021.12.118.

35. G. A. Elsammak, A. Talaat, and S. Reda, "The Possible Ameliorative Role of Lycopene on Tributyltin Induced Thyroid Damage in Adult Male Albino Rats (Histological, Immunohistochemical and Biochemical Study)," *Ultrastructural Pathology* 47 (2023): 324–338, https://doi.org/10.1080/01913123.2023.2205922.

36. S. Hanaoka, K. Ishida, S. Tanaka, et al., "Tributyltin Induces Epigenetic Changes and Decreases the Expression of Nuclear Respiratory Factor-1," *Metallomics* 10 (2018): 337–345, https://doi.org/10.1039/C7MT00290D.

37. S. Yamada, M. Asanagi, N. Hirata, H. Itagaki, Y. Sekino, and Y. Kanda, "Tributyltin Induces Mitochondrial Fission Through Mfn1 Degradation in Human Induced Pluripotent Stem Cells," *Toxicology In Vitro* 34 (2016): 257–263, https://doi.org/10.1016/j.tiv.2016.04.013.

38. S. Mitra, R. Gera, W. A. Siddiqui, and S. Khandelwal, "Tributyltin Induces Oxidative Damage, Inflammation and Apoptosis via Disturbance in Blood–Brain Barrier and Metal Homeostasis in Cerebral Cortex of Rat Brain: An In Vivo and In Vitro Study," *Toxicology* 310 (2013): 39–52, https://doi.org/10.1016/j.tox.2013.05.011.

39. K. Ishida, T. Saiki, K. Umeda, et al., "Prenatal Exposure to Tributyltin Decreases GluR2 Expression in the Mouse Brain," *Biological & Pharmaceutical Bulletin* 40 (2017): 1121–1124, https://doi.org/10.1248/bpb.b17-00209.

40. S. Fross, C. Mansel, M. McCormick, and B. P. S. Vohra, "Tributyltin Alters Calcium Levels, Mitochondrial Dynamics, and Activates Calpains Within Dorsal Root Ganglion Neurons," *Toxicological Sciences* 180 (2021): 342–355, https://doi.org/10.1093/toxsci/kfaa193.

41. X. Zheng, L. Boyer, M. Jin, et al., "Alleviation of Neuronal Energy Deficiency by mTOR Inhibition as a Treatment for Mitochondria-Related Neurodegeneration," *eLife* 5 (2016): e13378, https://doi.org/10.7554/eLife.13378.

42. S. M. Greenwood, S. M. Mizielinska, B. G. Frenguelli, J. Harvey, and C. N. Connolly, "Mitochondrial Dysfunction and Dendritic Beading During Neuronal Toxicity," *Journal of Biological Chemistry* 282 (2007): 26235–26244, https://doi.org/10.1074/jbc.M704488200.

43. F. Bao, H. Shi, M. Gao, et al., "Polybrene Induces Neural Degeneration by Bidirectional Ca^{2+} Influx-Dependent Mitochondrial and ER–Mitochondrial Dynamics," *Cell Death & Disease* 9 (2018): 966, https://doi.org/10.1038/s41419-018-1009-8.

44. S. Yamada, Y. Kubo, D. Yamazaki, et al., "Tributyltin Inhibits Neural Induction of Human Induced Pluripotent Stem Cells," *Scientific Reports* 8 (2018): 12155, https://doi.org/10.1038/s41598-018-30615-2.

45. H. Chiu, R. Yang, T. Weng, C. Y. Chiu, K. C. Lan, and S. H. Liu, "A Ubiquitous Endocrine Disruptor Tributyltin Induces Muscle Wasting and Retards Muscle Regeneration," *Journal of Cachexia, Sarcopenia and Muscle* 14 (2023): 167–181, https://doi.org/10.1002/jcsm.13119.

46. Y. Nakatsu, Y. Kotake, T. Takishita, and S. Ohta, "Long-Term Exposure to Endogenous Levels of Tributyltin Decreases GluR2 Expression and Increases Neuronal Vulnerability to Glutamate," *Toxicology and Applied Pharmacology* 240 (2009): 292–298, https://doi.org/10.1016/j.taap.2009.06.024.

47. K. Oyanagi, T. Tashiro, and T. Negishi, "Cell-Type-Specific and Differentiation-Status-Dependent Variations in Cytotoxicity of Tributyltin in Cultured Rat Cerebral Neurons and Astrocytes," *Journal of Toxicological Sciences* 40 (2015): 459–468, https://doi.org/10.2131/jts.40.459.

48. P. Cocci, G. Mosconi, and F. A. Palermo, "Effects of Tributyltin on Retinoid X Receptor Gene Expression and Global DNA Methylation During Intracapsular Development of the Gastropod Tritia Mutabilis (Linnaeus, 1758)," *Environmental Toxicology and Pharmacology* 88 (2021): 103753, https://doi.org/10.1016/j.etap.2021.103753.

49. H. Cai, M. Chen, Y. Gao, et al., "Transgenerational Effects and Mechanisms of Tributyltin Exposure on Neurodevelopment in the Male Offspring of Rats," *Environmental Science & Technology* 57 (2023): 10201–10210, https://doi.org/10.1021/acs.est.3c01546.

50. Y. Yavuz, D. O. Ozen, Z. Y. Erol, H. Goren, and B. Yilmaz, "Effects of Endocrine Disruptors on the Electrical Activity of Leptin Receptor Neurons in the Dorsomedial Hypothalamus and Anxiety-Like Behavior in Male Mice," *Environmental Pollution* 324 (2023): 121366, https://doi.org/10.1016/j.envpol.2023.121366.

51. Y. M. Kim, J. J. Lee, S.-K. Park, et al., "Effects of Tributyltin Acetate on Dopamine Biosynthesis and L-DOPA-Induced Cytotoxicity in PC12 Cells," *Archives of Pharmacal Research* 30 (2007): 858–865, https://doi.org/10.1007/BF02978837.

52. X. Tu, Y.-W. Li, Q.-L. Chen, Y. J. Shen, and Z. H. Liu, "Tributyltin Enhanced Anxiety of Adult Male Zebrafish Through Elevating Cortisol Level and Disruption in Serotonin, Dopamine and Gamma-Aminobutyric Acid Neurotransmitter Pathways," *Ecotoxicology and Environmental Safety* 203 (2020): 111014, https://doi.org/10.1016/j.ecoenv.2020.111014.

53. K. Nakayama, Y. Oshima, T. Tachibana, M. Furuse, and T. Honjo, "Alteration of Monoamine Concentrations in the Brain of Medaka,*Oryzias latipes*, Exposed to Tributyltin," *Environmental Toxicology* 22 (2007): 53–57, https://doi.org/10.1002/tox.20233.

54. H. S. Elsabbagh, S. Z. Moussa, and O. S. El-Tawil, "Neurotoxicologic Sequelae of Tributyltin Intoxication in Rats," *Pharmacological Research* 45 (2002): 201–206, https://doi.org/10.1006/phrs.2001.0909.

55. S. Mitra, W. A. Siddiqui, and S. Khandelwal, "Differential Susceptibility of Brain Regions to Tributyltin Chloride Toxicity," *Environmental Toxicology* 30 (2015): 1393–1405, https://doi.org/10.1002/tox.22009.

56. M. Ema, T. Itami, and H. Kawasaki, "Behavioral Effects of Acute Exposure to Tributyltin Chloride in Rats," *Neurotoxicology and Teratology* 13 (1991): 489–493, https://doi.org/10.1016/0892-0362(91)90054-Z.

57. J. P. O'Callaghan and D. B. Miller, "Acute Exposure of the Neonatal Rat to Tributyltin Results in Decreases in Biochemical Indicators of Synaptogenesis and Myelinogenesis," *Journal of Pharmacology and Experimental Therapeutics* 246 (1988): 394–402.

58. V. S. Ten, "Mitochondrial Dysfunction in Alveolar and White Matter Developmental Failure in Premature Infants," *Pediatric Research* 81 (2017): 286–292, https://doi.org/10.1038/pr.2016.216.

59. M. Zirngibl, P. Assinck, A. Sizov, A. V. Caprariello, and J. R. Plemel, "Oligodendrocyte Death and Myelin Loss in the Cuprizone Model: An Updated Overview of the Intrinsic and Extrinsic Causes of Cuprizone Demyelination," *Molecular Neurodegeneration* 17 (2022): 34, https://doi.org/10.1186/s13024-022-00538-8.

60. J. Kochmanski, M. Virani, N. C. Kuhn, et al., "Developmental Origins of Parkinson's Disease Risk: Perinatal Exposure to the Organochlorine Pesticide Dieldrin Leads to Sex-Specific DNA Modifications in Critical Neurodevelopmental Pathways in the Mouse Midbrain," *Toxicological Sciences* 201 (2024): 263–281, https://doi.org/10.1093/toxsci/kfae091.

61. G. Ponti, E. Bo, B. Bonaldo, et al., "Perinatal Exposure to Tributyltin Affects Feeding Behavior and Expression of Hypothalamic Neuropeptide Y in the Paraventricular Nucleus of Adult Mice," *Journal of Anatomy* 242 (2023): 235–244, https://doi.org/10.1111/joa.13766.

62. Y. Kotake, "Molecular Mechanisms of Environmental Organotin Toxicity in Mammals," *Biological & Pharmaceutical Bulletin* 35 (2012): 1876–1880, https://doi.org/10.1248/bpb.b212017.

63. S. Mitra, W. A. Siddiqui, and S. Khandelwal, "Early Cellular Responses Against Tributyltin Chloride Exposure in Primary Cultures Derived From Various Brain Regions," *Environmental Toxicology and Pharmacology* 37 (2014): 1048–1059, https://doi.org/10.1016/j.etap.2014.03.020.